Frequency-Coupled Impedance Modeling of Virtual Synchronous Generators

Kai Shi, Yu Wang, Yuxin Sun, Peifeng Xu, and Feng Gao

***Abstract*—The impedance of the virtual synchronous generator (VSG) is an effective method to analyze the dynamic interactions between the VSG and the grid. For the existence of power controllers and asymmetric inner-loop controllers in the d- and q-axis, there are couplings in the output sequence impedance of VSG. Although the couplings are relatively small, they still have a significant impact on the stability performance. However, there is no result published on this aspect up to now. To bridge this gap, a sequence impedance model based on harmonic linearization is established in this paper, which explicitly reveals the mirror frequency effect (MFE) in VSG. Subsequently, the relationships between the power controllers and the MFE are demonstrated. Finally, simulation results verify the feasibility and correctness of the theoretical analysis presented above.**

***Index Terms*—Virtual synchronous generator, stability analysis, power controllers, sequence impedance model, mirror frequency effect.**

I. Introduction

With the energy crisis and environmental destruction being prominent, the renewable energy and distributed power generation have received more and more attention in the world. A significant share of conventional fossil fuel-based power plants has been replaced with renewable energy resources. Unlike the case that the rotating parts of synchronous machines inherently provide inertia to the system, the application of a large number of power electronic converters makes the whole power system characterized by low inertia [1]. Power electronics have faster dynamics than conventional controllers for both active and reactive power support, meanwhile the unexpected issue on the frequency stability of power system is introduced for the lack of physical inertia [2], [3]. To deal with this problem, the virtual synchronous generator (VSG) technology was proposed and put into practice in the European project "VSYNC" [4]. It emulates the behavior of a traditional synchronous generator (SG) to provide adjustable inertia and damping as well as frequency and voltage support, which improves the permeability of distributed generation. At present, the practical applications of VSG have involved a variety of fields such as photovoltaic power plants [5], AC/DC microgrids [6], and wind power generation [7].

Nevertheless, some undesirable phenomenons such as synchronous frequency resonance, synchronous instability, and the low-frequency oscillation problem may also occur in VSG dominated power systems [8]–[11], which could degrade the performance of VSG and even bring in the instability of the system. The impedance model has been developed to address the stability challenges in VSG. In [12], [13], the state-space model based on small-signal approach was applied to analyze the control parameters by the eigenvalue and sensitivity. But there were too many variables involved. For instance, the small-signal model of the virtual synchronous machine (VSM) in [12] had 19 state variables, which gave 19 eigenvalues for this system. When the parallel units are considered, the order of system will be multiplied up, which would challenge the model feasibility and controller calculation. In [14], [15], a small-signal model of VSG was built in synchronous rotating reference frames (SRRFs). However, it cannot be used when AC system is unbalanced since the steady operation point of the small-signal system will no longer be DC constant. The harmonic linearization method [16] overcomes the above limitations by modeling three-phase impedance directly in the phase domain. The calculated impedance can handle both balanced and unbalanced systems, has clear physical interpretations and can be directly measured. So far, the method has been applied to model output impedance of various nonlinear systems. In [17], the sequence impedance model of VSG did not involve inner loops control. In [18], the VSG was decoupled into positive- and negative-sequence subsystems without considering the mirror frequency effect (MFE) [19].

In the existing impedance model, the inner loops of VSG are assumed to be identical. However, the power loops and *dq*-axis components are closely related, and the change of control parameters will affect the degree of system asymmetry. Even in a balanced system, positive- and negative-sequence will be coupled due to the coupling terms. The disturbance generated by the power controllers has great influence on the error of coordinate transformation. In this case, VSG cannot be assumed to be a mirror frequency decoupled (MFD) system, otherwise it would lead to an erroneous of the equivalent impedance. The normal Nyquist criterion is no longer applicable, and the generalized Nyquist criterion (GNC) should be utilized instead [20].

Manuscript received August 3, 2020; revised November 9, 2020; accepted December 27, 2020. Date of publication January 11, 2021; date of current version June 18, 2021. This work was supported in part by the National Natural Science Foundation of China under Grant 51407085, in part by National Key R&D Program of China under Grant 2017YFB0103200, and in part by the Project Funded by the Priority Academic Program Development of Jiangsu Higher Education Institution. Paper no. TPWRS-01306-2020. *(Corresponding author: Yuxin Sun.)*

The authors are with the School of Electrical and Information Engineering, Jiangsu University, Zhenjiang 212013, China (e-mail: shikai80614@163.com; wyu0214@foxmail.com; syx4461@ujs.edu.cn; xupeifeng2003@126.com; 997687789@qq.com).

Color versions of one or more figures in this article are available at https://doi.org/10.1109/TPWRS.2021.3050568.

Digital Object Identifier 10.1109/TPWRS.2021.3050568

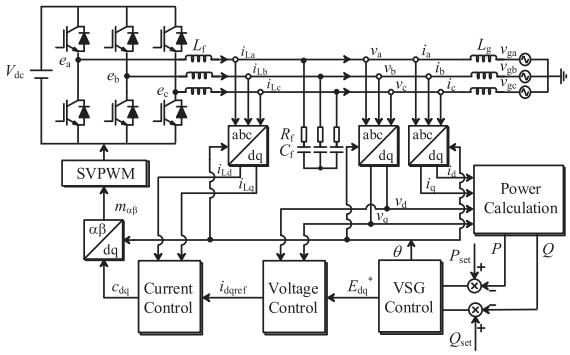

Fig. 1. Topology block diagram of VSG.

To explicitly reveal the MFE brought by the power controllers and inner-loop controllers in the VSG, a sequence impedance model is deduced by harmonic linearization in this paper. The impedance-based stability criterion is used to analyze which factors are closely related to the MFE and further investigate their impacts on the system stability. The close correlations between the power loops and coupling terms are discussed thoroughly, and subsequently validated in time domain simulations under different conditions. The results show that the MFE plays an important role in stability analysis and cannot be ignored.

II. Description Of VSG

Fig. 1 illustrates the topology of the VSG. In Fig. 1, $V_{\rm dc}$ is the DC-side voltage of VSG and can be regarded as a constant; $e_{\rm a}$, $e_{\rm b}$ and $e_{\rm c}$ are the inner electric potentials of VSG; $i_{\rm La}$, $i_{\rm Lb}$ and $i_{\rm Lc}$ are the output currents of VSG; $i_{\rm a}$, $i_{\rm b}$ and $i_{\rm c}$ are the grid-connected currents; $v_{\rm a}$, $v_{\rm b}$ and $v_{\rm c}$ are the output terminal voltages of VSG; $L_{\rm f}$, $C_{\rm f}$ and $R_{\rm f}$ are the filter inductance, filter capacitance and damping resistance respectively; $L_{\rm g}$ is the inductance on the grid side; $v_{\rm ga}$, $v_{\rm gb}$ and $v_{\rm gc}$ are the grid voltages.

Fig. 2 depicts the specific control diagram of the VSG. The active and reactive power control loops of VSG can imitate the operation principles of mechanical and electrical part of a real SG respectively. And the mathematical model of the active and reactive power controller of VSG can be expressed as follows:

$$T_{\rm set} + (\omega_n - \omega_v)D_{\rm p} - T_{\rm e} = Js\omega_v \tag{1}$$

$$T_{\rm e} = \frac{P_{\rm e}}{\omega_v} \approx \frac{P_e}{\omega_n} \tag{2}$$

$$T_{set} = \frac{P_{set}}{\omega_{\rm v}} \approx \frac{P_{set}}{\omega_{\rm n}} \tag{3}$$

$$\omega_{\rm v} = s\theta \tag{4}$$

$$Q_{set} + (V_0 - V)D_q - Q_e = KsE_m \tag{5}$$

where J and K are the virtual moment of inertia and voltage coefficient respectively; $\omega_{\rm v}$ and $\omega_{\rm n}$ are the output angular frequency of VSG and the rated angular frequency of the grid respectively; $T_{\rm set}$ and $T_{\rm e}$ are the reference torque and the electromagnetic toque respectively; $D_{\rm p}$ and $D_{\rm q}$ are the damping and the voltage-drooping coefficient respectively; $P_{\rm set}$ and $Q_{\rm set}$ are the active and reactive power reference; V_0, V, and $E_{\rm m}$ are the amplitudes of the rated voltage, the output voltage, and the inner electric potential respectively.

The instantaneous output active and reactive power of VSG can be calculated as

$$\begin{cases} P_{\rm e} = 1.5(v_{\rm d}i_{\rm d} + v_{\rm q}i_{\rm q}) \\ Q_{\rm e} = 1.5(v_{\rm q}i_{\rm d} - v_{\rm d}i_{\rm q}) \end{cases} \tag{6}$$

where $v_{\rm d}$ and $i_{\rm d}$ are the output voltage and current on d-axis respectively, and $v_{\rm q}$ and $i_{\rm q}$ are the output voltage and current on q-axis respectively.

The modulation wave of VSG is determined by the active and reactive power loop, and the voltage of the modulation wave can be expressed as follows:

$$\begin{cases} e_{\rm am} = E_{\rm m}\sin\theta \\ e_{\rm bm} = E_{\rm m}\sin\left(\theta - \frac{2}{3}\pi\right) \\ e_{\rm cm} = E_{\rm m}\sin\left(\theta + \frac{2}{3}\pi\right) \end{cases} \tag{7}$$

where $e_{\rm am}$, $e_{\rm bm}$ and $e_{\rm cm}$ are the three-phase modulation waves of VSG.

As shown in Fig. 1, the relationships among the inner electric potential, the output terminal voltage and the output current of VSG can be obtained as follows:

$$\begin{bmatrix} e_{\rm a} \\ e_{\rm b} \\ e_{\rm c} \end{bmatrix} = \left(\frac{L_{\rm f}C_{\rm f}s^2}{1 + C_{\rm f}R_{\rm f}s} + 1\right)\begin{bmatrix} v_{\rm a} \\ v_{\rm b} \\ v_{\rm c} \end{bmatrix} + L_{\rm f}s\begin{bmatrix} i_{\rm a} \\ i_{\rm b} \\ i_{\rm c} \end{bmatrix} \tag{8}$$

III. Mirror Frequency Effect in VSG

Since the MFE cannot be neglected due to *P*/*Q* controls and *dq* controls in the VSG [21], a small signal at frequency $f_{\rm p}+f_1$ injected to the point of common coupling (PCC) will lead to a corresponding signal at frequency $f_{\rm p}-f_1$. The signals at frequency $f_{\rm p}+f_1$ and $f_{\rm p}-f_1$ are mirror-frequency signals and symmetric about the fundamental frequency f_1 [22], [23]. For clarity, the signals at frequency $f_{\rm p}+f_1$ are called "positive-sequence" signals and the signals at frequency $f_{\rm p}-f_1$ are called "negative-sequence" signals.

Mirror frequency coupling is introduced when the system includes the following [19]:

1) PLL;
2) converter current controllers with unequal structure and/or parameter values in the d- and q-axis;
3) dc-link voltage control systems;
4) active and reactive power controllers;
5) salient-pole synchronous machines.

Therefore, in the time domain, after adding the small-signal perturbations, the output terminal voltage and current of phase A can be expressed as follows:

$$\begin{aligned} v_a(t) = {} & V_1\cos(2\pi f_1 t) + V_p\cos(2\pi(f_p + f_1)t + \varphi_{\rm vp}) \\ & + V_n\cos(2\pi(f_{\rm p} - f_1)t + \varphi_{vn}) \end{aligned} \tag{9}$$

$$\begin{aligned} i_a(t) = {} & I_1\cos(2\pi f_1 t + \varphi_{i1}) + I_p\cos(2\pi(f_p{+}f_1)t + \varphi_{ip}) \\ & + I_n\cos(2\pi(f_p - f_1)t + \varphi_{in}) \end{aligned} \tag{10}$$

where V_1, $V_{\rm p}$ and $V_{\rm n}$ are the amplitudes of the fundamental voltage, the positive- and negative-sequence voltage perturbation respectively; I_1, $I_{\rm p}$ and $I_{\rm n}$ are the amplitudes of the fundamental

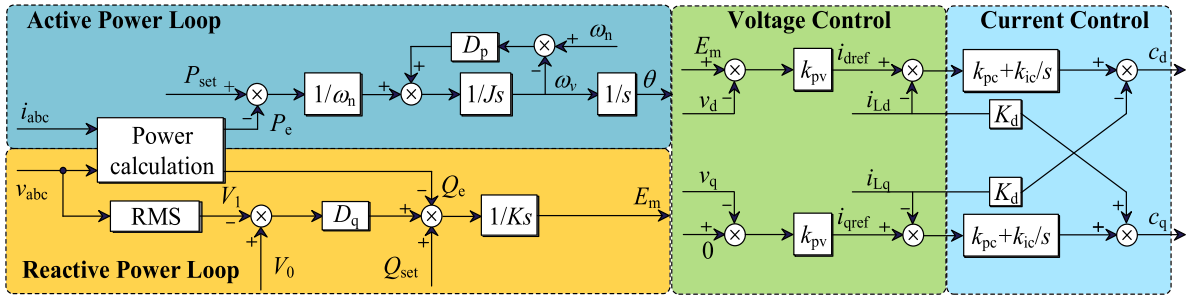

Fig. 2. Control block diagram of VSG.

current, the positive- and negative-sequence current response respectively; f_1, f_p and f_n are the fundamental frequency, the positive- and negative-sequence perturbation frequency respectively; φ_vp and φ_vn are the initial phase angles of the positive- and negative-sequence voltage perturbation respectively; φ_i1, φ_ip and φ_in are the initial phase angles of the fundamental current, positive- and negative-sequence current response respectively.

In the frequency domain, (9) and (10) can be written as follows:

$$\mathbf{V}_\mathrm{a}[f]=\begin{cases}\mathbf{V}_1, & f=\pm f_1\\ \mathbf{V}_\mathrm{p}, & f=\pm(f_\mathrm{p}+f_1)\\ \mathbf{V}_\mathrm{n}, & f=\pm(f_\mathrm{p}-f_1)\end{cases} \tag{11}$$

$$\mathbf{I}_\mathrm{a}[f]=\begin{cases}\mathbf{I}_1, & f=\pm f_1\\ \mathbf{I}_\mathrm{p}, & f=\pm(f_\mathrm{p}+f_1)\\ \mathbf{I}_\mathrm{n}, & f=\pm(f_\mathrm{p}-f_1)\end{cases} \tag{12}$$

where $\mathbf{V}_1=V_1/2$; $\mathbf{V}_\mathrm{p}=(V_\mathrm{p}/2)\mathrm{e}^{\pm\mathrm{j}\varphi\mathrm{vp}}$; $\mathbf{V}_\mathrm{n}=(V_\mathrm{n}/2)\mathrm{e}^{\pm\mathrm{j}\varphi\mathrm{vn}}$; $\mathbf{I}_1=(I_1/2)\mathrm{e}^{\pm\mathrm{j}\varphi\mathrm{i1}}$; $\mathbf{I}_\mathrm{p}=(I_\mathrm{p}/2)\mathrm{e}^{\pm\mathrm{j}\varphi\mathrm{ip}}$; $\mathbf{I}_\mathrm{n}=(I_\mathrm{n}/2)\mathrm{e}^{\pm\mathrm{j}\varphi\mathrm{in}}$.

The small-signal behavior of VSG from its ac terminals can be described by an admittance matrix as

$$\begin{bmatrix}I_\mathrm{p}(s+\mathrm{j}\omega_1)\\ I_\mathrm{n}(s-\mathrm{j}\omega_1)\end{bmatrix}=-\begin{bmatrix}Y_\mathrm{pp}(s) & Y_\mathrm{pn}(s)\\ Y_\mathrm{np}(s) & Y_\mathrm{nn}(s)\end{bmatrix}\begin{bmatrix}V_\mathrm{p}(s+\mathrm{j}\omega_1)\\ V_\mathrm{n}(s-\mathrm{j}\omega_1)\end{bmatrix} \tag{13}$$

As shown in the above equation, the diagonal elements Y_pp and Y_nn in the admittance matrix $\mathbf{Y}_\mathrm{PN}(\mathrm{s})$ correspond to the positive- and negative-sequence admittance respectively, while the non-diagonal elements reflect the frequency-coupling relationship in the VSG.

IV. Analytical Modelling

After the Park's transformation, the frequency-domain output voltage (11) and current (12) can be written as follows:

$$\mathbf{V}_\mathrm{d1}[f]=\begin{cases}V_1, & \mathrm{dc}\\ \mathbf{V}_\mathrm{p}+\mathbf{V}_\mathrm{n}, & f=\pm f_p\end{cases} \tag{14}$$

$$\mathbf{V}_\mathrm{q1}[f]=\begin{cases}0, & \mathrm{dc}\\ \mp\mathrm{j}\mathbf{V}_\mathrm{p}\pm\mathrm{j}\mathbf{V}_\mathrm{n}, & f=\pm f_\mathrm{p}\end{cases} \tag{15}$$

$$\mathbf{I}_\mathrm{d1}[f]=\begin{cases}I_1\cos\varphi_\mathrm{i1}, & \mathrm{dc}\\ \mathbf{I}_\mathrm{p}+\mathbf{I}_\mathrm{n}, & f=\pm f_\mathrm{p}\end{cases} \tag{16}$$

$$\mathbf{I}_\mathrm{q1}[f]=\begin{cases}I_1\sin\varphi_\mathrm{i1}, & \mathrm{dc}\\ \mp\mathrm{j}\mathbf{I}_\mathrm{p}\pm\mathrm{j}\mathbf{I}_\mathrm{n}, & f=\pm f_\mathrm{p}\end{cases} \tag{17}$$

By substituting (14)-(17) into (6) and utilizing the frequency-domain convolution theorem, the active power and the reactive power in the frequency domain can be obtained as follows:

$$\mathbf{P}_\mathrm{e}[f]=\begin{cases}1.5V_1I_\mathrm{dr}, & \mathrm{dc}\\ 3(\mathbf{V}_1\mathbf{I}_\mathrm{p}+\mathbf{V}_1\mathbf{I}_\mathrm{n}+\mathbf{I}_1^*\mathbf{V}_\mathrm{p}+\mathbf{I}_1\mathbf{V}_\mathrm{n}), & f=\pm f_p\end{cases} \tag{18}$$

$$\mathbf{Q}_\mathrm{e}[f]=\begin{cases}-1.5V_1I_\mathrm{qr}, & \mathrm{dc}\\ 3(\pm\mathrm{j}\mathbf{V}_1\mathbf{I}_\mathrm{p}\mp\mathrm{j}\mathbf{V}_1\mathbf{I}_\mathrm{n}-\mathbf{I}_2^*\mathbf{V}_\mathrm{p}-\mathbf{I}_2\mathbf{V}_\mathrm{n}), & f=\pm f_p\end{cases} \tag{19}$$

where $\mathbf{I}_2=(I_1/2)\mathrm{e}^{\pm\mathrm{j}(\varphi\mathrm{i1}-\pi/2)}$, the superscript symbol "$*$" denotes the complex conjugate.

On the basis of the active power controller of the VSG in Fig. 2, the phase angle θ can be obtained as follows:

$$\theta=M(s)\left(\omega_\mathrm{n}D_\mathrm{p}+\frac{P_\mathrm{set}}{\omega_\mathrm{n}}-\frac{P_\mathrm{e}}{\omega_\mathrm{n}}\right) \tag{20}$$

where $M(s)=1/(Js^2+D_\mathrm{p}s)$.

By substituting (18) into (20), the expression of θ in the frequency domain can be obtained as follows:

$$\theta[f]=\begin{cases}M(s)[\omega_nD_\mathrm{p}+\frac{P_\mathrm{set}}{\omega_\mathrm{n}}-\frac{1.5V_1I_\mathrm{dr}}{\omega_n}], & \mathrm{dc}\\ -\frac{3M(s)}{\omega_\mathrm{n}}(\mathbf{V}_1\mathbf{I}_p+\mathbf{V}_1\mathbf{I}_n+\mathbf{I}_1^*\mathbf{V}_\mathrm{p}+\mathbf{I}_1\mathbf{V}_n), & f=\pm f_p\end{cases} \tag{21}$$

For the sake of the phase angle perturbation $\Delta\theta$, θ can be described as $\theta=\theta_1+\Delta\theta$, where θ_1 is the phase angle of the fundamental voltage, and $\Delta\theta$ is a small perturbation by the disturbance voltage. Thus, $\Delta\theta$ in the frequency domain can be obtained from (21) as follows:

$$\Delta\theta[f]=-\frac{3M(s)}{\omega_\mathrm{n}}(\mathbf{V}_1\mathbf{I}_p+\mathbf{V}_1\mathbf{I}_n+\mathbf{I}_1^*\mathbf{V}_\mathrm{p}+\mathbf{I}_1\mathbf{V}_\mathrm{n}),\ f=\pm f_p \tag{22}$$

Because $\Delta\theta$ is a small perturbation, $\sin\theta$ can be deduced by an approximate treatment as

$$\sin\theta=\sin(\theta_1+\Delta\theta)\approx\sin\theta_1+\Delta\theta\cos\theta_1 \tag{23}$$

Then, by substituting (22) into (23), $\sin\theta$ in the frequency domain can be further derived as follows:

$$\mathbf{sin}\theta[f]=\begin{cases}\mp\frac{\mathrm{j}}{2}, & f=\pm f_1\\ -\frac{3M(s\mp\mathrm{j}\omega_1)}{2\omega_\mathrm{n}}(\mathbf{V}_1\mathbf{I}_p+\mathbf{V}_1\mathbf{I}_n+\mathbf{I}_1^*\mathbf{V}_\mathrm{p}+\mathbf{I}_1\mathbf{V}_n), & f=\pm(f_\mathrm{p}+f_1)\\ -\frac{3M(s\pm\mathrm{j}\omega_1)}{2\omega_\mathrm{n}}(\mathbf{V}_1\mathbf{I}_p+\mathbf{V}_1\mathbf{I}_\mathrm{n}+\mathbf{I}_1^*\mathbf{V}_p+\mathbf{I}_1\mathbf{V}_n), & f=\pm(f_p-f_1)\end{cases} \tag{24}$$

In the same way, based on the reactive power controller of the VSG, E_m can be obtained as follows:

$$E_m=D(s)(Q_{set}-Q_e)+V_0 \tag{25}$$

where $D(s)=1/(Ks+D_\mathrm{q})$.

By substituting (19) into (25), E_m in the frequency domain can be expressed as follows:

$$\mathbf{E}_m[f]=\begin{cases}V_0, & \mathrm{dc}\\ -3D(s)(\pm\mathrm{j}\mathbf{V}_1\mathbf{I}_\mathrm{p}\mp\mathrm{j}\mathbf{V}_1\mathbf{I}_n-\mathbf{I}_2^*\mathbf{V}_p-\mathbf{I}_2\mathbf{V}_n), & f=\pm f_\mathrm{p}\end{cases} \tag{26}$$

Set the d- and q-axis reference voltage as

$$\begin{cases}v_\mathrm{dref}=E_\mathrm{m}\\ v_\mathrm{qref}=0\end{cases} \tag{27}$$

When $\Delta\theta$ is considered, the output voltage in the SRRF is as follows:

$$\begin{cases}v_d=v_{d1}+\Delta\theta v_{q1}\\ v_\mathrm{q}=-\Delta\theta v_\mathrm{d1}+v_{q1}\end{cases} \tag{28}$$

Based on (14)-(15) and (28), the output voltages in the frequency domain can be derived as follows:

$$\mathbf{V}_\mathrm{d}[f]=\begin{cases}V_1, & \mathrm{dc}\\ \mathbf{V}_\mathrm{p}+\mathbf{V}_\mathrm{n}, & f=\pm f_p\end{cases} \tag{29}$$

$$\mathbf{V}_\mathrm{q}[f]=\begin{cases}0, & \mathrm{dc}\\ \frac{3M(s)V_1}{\omega_\mathrm{n}}(\mathbf{V}_1\mathbf{I}_p+\mathbf{V}_1\mathbf{I}_n+\mathbf{I}_1^*\mathbf{V}_\mathrm{p}+\mathbf{I}_1\mathbf{V}_\mathrm{n}) & \\ \mp\mathrm{j}\mathbf{V}_\mathrm{p}\pm\mathrm{j}\mathbf{V}_\mathrm{n}, & f=\pm f_\mathrm{p}\end{cases} \tag{30}$$

Similarly, the output currents are as follows:

$$\mathbf{I}_\mathrm{d}[f]=\begin{cases}I_1\cos\varphi_\mathrm{i1}, & \mathrm{dc}\\ \mathbf{I}_\mathrm{p}+\mathbf{I}_\mathrm{n}-\frac{3M(s)I_\mathrm{qr}}{\omega_\mathrm{n}}(\mathbf{V}_1\mathbf{I}_p+\mathbf{V}_1\mathbf{I}_n+\mathbf{I}_1^*\mathbf{V}_\mathrm{p}+\mathbf{I}_1\mathbf{V}_\mathrm{n}), & \\ f=\pm f_\mathrm{p}\end{cases} \tag{31}$$

$$\mathbf{I}_\mathrm{q}[f]=\begin{cases}I_1\sin\varphi_\mathrm{i1}, & \mathrm{dc}\\ \mp\mathrm{j}\mathbf{I}_\mathrm{p}\pm\mathrm{j}\mathbf{I}_\mathrm{n}+\frac{3M(s)I_\mathrm{dr}}{\omega_\mathrm{n}} & \\ (\mathbf{V}_1\mathbf{I}_p+\mathbf{V}_1\mathbf{I}_n+\mathbf{I}_1^*\mathbf{V}_\mathrm{p}+\mathbf{I}_1\mathbf{V}_\mathrm{n}), & f=\pm f_p\end{cases} \tag{32}$$

Combined with the voltage given in the (27), the output of the voltage loop, namely the input of the current inner loop, can be obtained as follows:

$$\begin{cases}i_\mathrm{dref}=k_\mathrm{pv}(v_\mathrm{dref}-v_\mathrm{d})\\ i_\mathrm{qref}=k_\mathrm{pv}(v_\mathrm{qref}-v_q)\end{cases} \tag{33}$$

where k_pv is proportional gain of voltage controller.

In the same way, the output of the current inner loop can be obtained as follows:

$$\begin{cases}c_\mathrm{d}=G_\mathrm{i}(s)(i_\mathrm{dref}-i_\mathrm{Ld})-K_di_\mathrm{Lq}\\ c_q=G_\mathrm{i}(s)(i_\mathrm{qref}-i_\mathrm{Lq})+K_di_\mathrm{Ld}\end{cases} \tag{34}$$

where G_i(s) is the transfer function of the PI current regulator; K_d is decoupling term.

Hence, the expressions of c_dq in the frequency domain can be derived as (39)-(40).

According to the inverse Park's transformation, c_abc in the stationary frame can be obtained as follows:

$$\begin{aligned}\begin{bmatrix}c_\mathrm{a}\\ c_b\\ c_c\end{bmatrix}&=T^{-1}(\theta_{PLL})\begin{bmatrix}c_\mathrm{d}\\ c_q\\ 0\end{bmatrix}\\ &\approx T^{-1}(\theta_1)\begin{bmatrix}1 & -\Delta\theta & 0\\ \Delta\theta & 1 & 0\\ 0 & 0 & 1\end{bmatrix}\begin{bmatrix}c_\mathrm{d}\\ c_q\\ 0\end{bmatrix}\end{aligned} \tag{35}$$

where

$$T^{-1}(\theta_1)=\begin{bmatrix}\cos\theta_1 & -\sin\theta_1 & 1/2\\ \cos(\theta_1-2\pi/3) & -\sin(\theta_1-2\pi/3) & 1/2\\ \cos(\theta_1+2\pi/3) & -\sin(\theta_1+2\pi/3) & 1/2\end{bmatrix} \tag{36}$$

And c_d1 and c_q1 are as follows:

$$\begin{bmatrix}c_\mathrm{d1}\\ c_{q1}\\ 0\end{bmatrix}\approx\begin{bmatrix}1 & -\Delta\theta & 0\\ \Delta\theta & 1 & 0\\ 0 & 0 & 1\end{bmatrix}\begin{bmatrix}c_\mathrm{d}\\ c_q\\ 0\end{bmatrix} \tag{37}$$

That is to say,

$$\begin{cases}c_{d1}=c_d-\Delta\theta c_\mathrm{q}\\ c_\mathrm{q1}=\Delta\theta c_d+c_\mathrm{q}\end{cases} \tag{38}$$

Based on (22) and (39)-(40), as shown at the bottom of the next page, c_dq1 in the frequency domain can be derived as (41)-(42), as shown at the bottom of the next page. Furthermore, the inner electric potential in the frequency domain can be obtained as (43), as shown at bottom of the next page. After that, based on (8) and (43), the impedance can be derived as (44)-(47), as shown at the bottom of the next page, where

$$\begin{cases}\mathbf{A}=\mathbf{V}_1\mathbf{I}_p+\mathbf{V}_1\mathbf{I}_n+\mathbf{I}_1^*\mathbf{V}_\mathrm{p}+\mathbf{I}_1\mathbf{V}_\mathrm{n}\\ \mathbf{B}=\pm\mathrm{j}\mathbf{V}_1\mathbf{I}_\mathrm{p}\mp\mathrm{j}\mathbf{V}_1\mathbf{I}_n-\mathbf{I}_2^*\mathbf{V}_p-\mathbf{I}_2\mathbf{V}_n\\ Y_\mathrm{c}(s)=\frac{C_\mathrm{f}s}{1+R_\mathrm{f}C_\mathrm{f}s}\\ Z_\mathrm{f}(s)=\frac{L_fC_\mathrm{f}s^2}{1+R_\mathrm{f}C_\mathrm{f}s}+1\end{cases} \tag{48}$$

The relationships between the voltage and the current are as follows:

$$V_\mathrm{p}=\begin{cases}-Z_\mathrm{pp}I_\mathrm{p}, & f=f_\mathrm{p}+f_1,\ Pos.\\ -Z_\mathrm{pn}I_n, & f=f_\mathrm{p}-f_1,\ Neg.\end{cases} \tag{49}$$

$$V_\mathrm{n}=\begin{cases}-Z_{np}I_\mathrm{p}, & f=f_\mathrm{p}+f_1,\ Pos.\\ -Z_\mathrm{nn}I_n, & f=f_\mathrm{p}-f_1,\ Neg.\end{cases} \tag{50}$$

And the admittance model can be derived from the output impedance matrix as follows:

$$\begin{bmatrix} Y_{pp} & Y_{\mathrm{pn}} \\ Y_{np} & Y_{\mathrm{nn}} \end{bmatrix} = \begin{bmatrix} \frac{Z_{\mathrm{nn}}}{Z_{\mathrm{pp}}Z_{nn}-Z_{pn}Z_{np}} & \frac{-Z_{\mathrm{pn}}}{Z_{\mathrm{pp}}Z_{nn}-Z_{pn}Z_{np}} \\ \frac{-Z_{\mathrm{np}}}{Z_{\mathrm{pp}}Z_{nn}-Z_{pn}Z_{np}} & \frac{Z_{\mathrm{pp}}}{Z_{\mathrm{pp}}Z_{nn}-Z_{pn}Z_{np}} \end{bmatrix} \tag{51}$$

V. Simulation Verification

In order to verify the proposed mathematical model, a time-domain simulation model is built in Matlab/Simulink according to the VSG structure in Fig. 1. The system parameters are provided in Table I.

Fig. 3 depicts the frequency responses of output impedance. It is obvious that the impedance measurement results are in good accordance with the theoretical results, which verifies the correctness of the sequence impedance model. It can be found that the amplitudes of the four curves near the fundamental frequency are basically the same. This implies that the off-diagonal elements cannot be ignored.

Fig. 4 plots the impedance responses of different virtual inertia. It can be found from the impedance curves that the adjustment of *J* has no fundamental change to the output impedance of the system. Overall, the variation of *J* has a weak effect on the output impedance. However, there is obvious amplitude and

$$C_{\mathrm{d}}[f] = \begin{cases} -G_{\mathrm{i}}(s)I_{\mathrm{dr}} - K_{\mathrm{d}}I_{\mathrm{qr}} - G_{\mathrm{i}}(s)Y_{\mathrm{c}}(s)V_1 & \mathrm{dc} \\ \left\{[-3D(s)\mathbf{B} - \mathbf{V}_{\mathrm{p}} - \mathbf{V}_{\mathrm{n}}]\,k_{pv} - \mathbf{I}_p - \mathbf{I}_n + \frac{3M(s)I_{\mathrm{qr}}\mathbf{A}}{\omega_{\mathrm{n}}}\right\} G_i(s) - K_{\mathrm{d}}\left[\mp \mathrm{j}\mathbf{I}_p \pm \mathrm{j}\mathbf{I}_n + \frac{3M(s)I_{\mathrm{dr}}\mathbf{A}}{\omega_{\mathrm{n}}}\right] \\ -G_{\mathrm{i}}(s)Y_{\mathrm{c}}(s)(\mathbf{V}_{\mathrm{p}} + \mathbf{V}_{\mathrm{n}}) - K_{\mathrm{d}}Y_{\mathrm{c}}(s)\left[\frac{3V_1M(s)\mathbf{A}}{\omega_{\mathrm{n}}} \mp \mathrm{j}\mathbf{V}_{\mathrm{p}} \pm \mathrm{j}\mathbf{V}_{\mathrm{n}}\right] & f = \pm f_{\mathrm{p}} \end{cases} \tag{39}$$

$$C_{\mathrm{q}}[f] = \begin{cases} -G_{\mathrm{i}}(s)I_{\mathrm{qr}} + K_{\mathrm{d}}I_{\mathrm{dr}} + K_{\mathrm{d}}Y_{\mathrm{c}}(s)V_1 & \mathrm{dc} \\ \left\{\left[-\frac{3V_1M(s)\mathbf{A}}{\omega_{\mathrm{n}}} \pm \mathrm{j}\mathbf{V}_{\mathrm{p}} \mp \mathrm{j}\mathbf{V}_{\mathrm{n}}\right] k_{pv} \pm \mathrm{j}\mathbf{I}_p \mp \mathrm{j}\mathbf{I}_n - \frac{3M(s)I_{\mathrm{dr}}\mathbf{A}}{\omega_{\mathrm{n}}}\right\} G_i(s) + K_{\mathrm{d}}(\mathbf{I}_p + \mathbf{I}_n - \frac{3M(s)I_{\mathrm{qr}}\mathbf{A}}{\omega_{\mathrm{n}}}) \\ +K_{\mathrm{d}}Y_{\mathrm{c}}(s)(\mathbf{V}_{\mathrm{p}} + \mathbf{V}_{\mathrm{n}}) - G_{\mathrm{i}}(s)Y_{\mathrm{c}}(s)\left[\frac{3V_1M(s)\mathbf{A}}{\omega_{\mathrm{n}}} \mp \mathrm{j}\mathbf{V}_{\mathrm{p}} \pm \mathrm{j}\mathbf{V}_{\mathrm{n}}\right] & f = \pm f_{\mathrm{p}} \end{cases} \tag{40}$$

$$C_{\mathrm{d1}}[f] = \begin{cases} -G_{\mathrm{i}}(s)I_{\mathrm{dr}} - K_{\mathrm{d}}I_{\mathrm{qr}} - G_{\mathrm{i}}(s)Y_{\mathrm{c}}(s)V_1 & \mathrm{dc} \\ \{[-3D(s)\mathbf{B} - \mathbf{V}_{\mathrm{p}} - \mathbf{V}_{\mathrm{n}}]\,k_{pv} - \mathbf{I}_p - \mathbf{I}_n\}\,G_i(s) + \mathrm{j}K_{\mathrm{d}}\,(\pm\mathbf{I}_p \mp \mathbf{I}_n) - G_{\mathrm{i}}(s)Y_{\mathrm{c}}(s)(\mathbf{V}_{\mathrm{p}} + \mathbf{V}_{\mathrm{n}}) \\ +\mathrm{j}K_{\mathrm{d}}Y_{\mathrm{c}}(s)(\pm\mathbf{V}_{\mathrm{p}} \mp \mathbf{V}_{\mathrm{n}})f = \pm f_{\mathrm{p}} \end{cases} \tag{41}$$

$$C_{\mathrm{q1}}[f] = \begin{cases} -G_{\mathrm{i}}(s)I_{\mathrm{qr}} + K_{\mathrm{d}}I_{\mathrm{dr}} + K_{\mathrm{d}}Y_{\mathrm{c}}(s)V_1 & \mathrm{dc} \\ \left\{\left[-\frac{3V_1M(s)\mathbf{A}}{\omega_{\mathrm{n}}} \pm \mathrm{j}\mathbf{V}_{\mathrm{p}} \mp \mathrm{j}\mathbf{V}_{\mathrm{n}}\right] k_{pv} \pm \mathrm{j}\mathbf{I}_p \mp \mathrm{j}\mathbf{I}_n\right\} G_i(s) + \mathrm{j}G_{\mathrm{i}}(s)Y_{\mathrm{c}}(s)(\pm\mathbf{V}_{\mathrm{p}} \mp \mathbf{V}_{\mathrm{n}}) + K_{\mathrm{d}}Y_{\mathrm{c}}(s)(\mathbf{V}_{\mathrm{p}} + \mathbf{V}_{\mathrm{n}}) \\ +K_{\mathrm{d}}\,(\mathbf{I}_p + \mathbf{I}_n) & f = \pm f_{\mathrm{p}} \end{cases} \tag{42}$$

$$\mathbf{C}_a[f] = \begin{cases} \frac{-G_{\mathrm{i}}(s\mp\mathrm{j}\omega_1)I_{\mathrm{dr}} - K_{\mathrm{d}}I_{\mathrm{qr}} - G_{\mathrm{i}}(s\mp\mathrm{j}\omega_1)Y_{\mathrm{c}}(s\pm\mathrm{j}\omega_1)V_1}{2} \pm \mathrm{j}\frac{[-G_{\mathrm{i}}(s\pm\mathrm{j}\omega_1)I_{\mathrm{qr}} + K_{\mathrm{d}}I_{\mathrm{dr}} + K_{\mathrm{d}}Y_{\mathrm{c}}(s\mp\mathrm{j}\omega_1)V_1]}{2} & f = \pm f_1 \\ \frac{-3k_{pv}G_i(s\mp\mathrm{j}\omega_1)D(s\mp\mathrm{j}\omega_1)\mathbf{B}}{2} - \frac{\mathrm{j}3k_{pv}G_i(s\mp\mathrm{j}\omega_1)V_1M(s\mp\mathrm{j}\omega_1)\mathbf{A}}{2\omega_{\mathrm{n}}} - [G_i(s \mp \mathrm{j}\omega_1) - \mathrm{j}K_{\mathrm{d}}]\,\mathbf{I}_p \\ -[G_{\mathrm{i}}(s \mp \mathrm{j}\omega_1)Y_{\mathrm{c}}(s \pm \mathrm{j}\omega_1) - \mathrm{j}K_{\mathrm{d}}Y_{\mathrm{c}}(s \pm \mathrm{j}\omega_1)]\,\mathbf{V}_{\mathrm{p}} - k_{pv}G_i(s \mp \mathrm{j}\omega_1)\mathbf{V}_{\mathrm{p}} & f = \pm(f_{\mathrm{p}} + f_1) \\ \frac{-3k_{pv}G_i(s\pm\mathrm{j}\omega_1)D(s\pm\mathrm{j}\omega_1)\mathbf{B}}{2} + \frac{\mathrm{j}3k_{pv}G_i(s\pm\mathrm{j}\omega_1)V_1M(s\pm\mathrm{j}\omega_1)\mathbf{A}}{2\omega_{\mathrm{n}}} - [G_i(s \pm \mathrm{j}\omega_1) + \mathrm{j}K_{\mathrm{d}}]\,\mathbf{I}_n \\ -[G_{\mathrm{i}}(s \pm \mathrm{j}\omega_1)Y_{\mathrm{c}}(s \mp \mathrm{j}\omega_1) + \mathrm{j}K_{\mathrm{d}}Y_{\mathrm{c}}(s \mp \mathrm{j}\omega_1)]\,\mathbf{V}_{\mathrm{n}} - k_{pv}G_i(s \pm \mathrm{j}\omega_1)\mathbf{V}_{\mathrm{n}} & f = \pm(f_{\mathrm{p}} - f_1) \end{cases} \tag{43}$$

$$\begin{aligned} Z_{\mathrm{pp}}(s) = {} & \left\{\left[\frac{-\mathrm{j}3k_{pv}G_i(s-\mathrm{j}\omega_1)V_1M(s-\mathrm{j}\omega_1)}{2\omega_{\mathrm{n}}} - \frac{\mathrm{j}3k_{pv}G_i(s-\mathrm{j}\omega_1)D(s-\mathrm{j}\omega_1)}{2}\right]\mathbf{V}_1 - G_i(s-\mathrm{j}\omega_1) + \mathrm{j}K_{\mathrm{d}} - L_{\mathrm{f}}(s+\mathrm{j}\omega_1)\right\} \\ & \times \left[\begin{array}{l} \frac{-\mathrm{j}3k_{pv}G_i(s-\mathrm{j}\omega_1)V_1M(s-\mathrm{j}\omega_1)}{2\omega_{\mathrm{n}}}\mathbf{I}_1^* + \frac{3k_{pv}G_i(s-\mathrm{j}\omega_1)D(s-\mathrm{j}\omega_1)}{2}\mathbf{I}_2^* - k_{pv}G_i(s-\mathrm{j}\omega_1) - G_{\mathrm{i}}(s-\mathrm{j}\omega_1)Y_{\mathrm{c}}(s+\mathrm{j}\omega_1) \\ +\mathrm{j}K_{\mathrm{d}}Y_{\mathrm{c}}(s+\mathrm{j}\omega_1) - Z_{\mathrm{f}}(s+\mathrm{j}\omega_1) \end{array}\right]^{-1} \end{aligned} \tag{44}$$

$$\begin{aligned} Z_{\mathrm{pn}}(s) = {} & \left[\frac{-\mathrm{j}3k_{pv}G_i(s-\mathrm{j}\omega_1)V_1M(s-\mathrm{j}\omega_1)}{2\omega_{\mathrm{n}}} + \frac{\mathrm{j}3k_{pv}G_i(s-\mathrm{j}\omega_1)D(s-\mathrm{j}\omega_1)}{2}\right]\mathbf{V}_1 \\ & \times \left[\begin{array}{l} \frac{-\mathrm{j}3k_{pv}G_i(s-\mathrm{j}\omega_1)V_1M(s-\mathrm{j}\omega_1)}{2\omega_{\mathrm{n}}}\mathbf{I}_1^* + \frac{3k_{pv}G_i(s-\mathrm{j}\omega_1)D(s-\mathrm{j}\omega_1)}{2}\mathbf{I}_2^* - k_{pv}G_i(s-\mathrm{j}\omega_1) - G_{\mathrm{i}}(s-\mathrm{j}\omega_1)Y_{\mathrm{c}}(s+\mathrm{j}\omega_1) \\ +\mathrm{j}K_{\mathrm{d}}Y_{\mathrm{c}}(s+\mathrm{j}\omega_1) - Z_{\mathrm{f}}(s+\mathrm{j}\omega_1) \end{array}\right]^{-1} \end{aligned} \tag{45}$$

$$\begin{aligned} Z_{\mathrm{np}}(s) = {} & \left[\frac{\mathrm{j}3k_{pv}G_i(s+\mathrm{j}\omega_1)VM(s+\mathrm{j}\omega_1)_1}{2\omega_{\mathrm{n}}} - \frac{\mathrm{j}3k_{pv}G_i(s+\mathrm{j}\omega_1)D(s+\mathrm{j}\omega_1)}{2}\right]\mathbf{V}_1 \\ & \times \left[\begin{array}{l} \frac{\mathrm{j}3k_{pv}G_i(s+\mathrm{j}\omega_1)V_1M(s+\mathrm{j}\omega_1)}{2\omega_{\mathrm{n}}}\mathbf{I}_1 + \frac{3k_{pv}G_i(s+\mathrm{j}\omega_1)D(s+\mathrm{j}\omega_1)}{2}\mathbf{I}_2 - k_{pv}G_i(s+\mathrm{j}\omega_1) - G_{\mathrm{i}}(s+\mathrm{j}\omega_1)Y_{\mathrm{c}}(s-\mathrm{j}\omega_1) \\ -\mathrm{j}K_{\mathrm{d}}Y_{\mathrm{c}}(s-\mathrm{j}\omega_1) - Z_{\mathrm{f}}(s-\mathrm{j}\omega_1) \end{array}\right]^{-1} \end{aligned} \tag{46}$$

$$\begin{aligned} Z_{\mathrm{nn}}(s) = {} & \left\{\left[\frac{\mathrm{j}3k_{pv}G_i(s+\mathrm{j}\omega_1)V_1M(s+\mathrm{j}\omega_1)}{2\omega_{\mathrm{n}}} + \frac{\mathrm{j}3k_{pv}G_i(s+\mathrm{j}\omega_1)D(s+\mathrm{j}\omega_1)}{2}\right]\mathbf{V}_1 - G_i(s+\mathrm{j}\omega_1) - \mathrm{j}K_{\mathrm{d}} - L_{\mathrm{f}}(s-\mathrm{j}\omega_1)\right\} \\ & \times \left[\begin{array}{l} \frac{\mathrm{j}3k_{pv}G_i(s+\mathrm{j}\omega_1)V_1M(s+\mathrm{j}\omega_1)}{2\omega_{\mathrm{n}}}\mathbf{I}_1 + \frac{3k_{pv}G_i(s+\mathrm{j}\omega_1)D(s+\mathrm{j}\omega_1)}{2}\mathbf{I}_2 - k_{pv}G_i(s+\mathrm{j}\omega_1) - G_{\mathrm{i}}(s+\mathrm{j}\omega_1)Y_{\mathrm{c}}(s-\mathrm{j}\omega_1) \\ -\mathrm{j}K_{\mathrm{d}}Y_{\mathrm{c}}(s-\mathrm{j}\omega_1) - Z_{\mathrm{f}}(s-\mathrm{j}\omega_1) \end{array}\right]^{-1} \end{aligned} \tag{47}$$

TABLE I
PARAMETERS OF VSG

Parameter	Value
Virtual inertia (J)	0.058 kg·m^2
VSG voltage coefficient (K)	6.5
Rated voltage amplitude (V_0)	311.3 V
Rated angular frequency (ω_n)	314.2 rad/s
Active, reactive power reference (P_{set}, Q_{set})	7 kW, 300 Var
P-f, Q-V Droop coefficient (D_p, D_q)	5, 320
Proportional gain of voltage controller (k_{pv})	1.2
Proportional gain of current controller (k_{pi})	6
Integral gain of current controller (k_{ii})	0.1
Virtual impedance (R_v, L_v)	0.05 Ω, 4 mH
DC voltage (V_{dc})	800 V
VSG switching frequency (f_n)	10kHz
Fundamental frequency (f_1)	50Hz
LC filter (L_f, C_f)	3 mH, 10 μF
Grid inductance (L_g)	10 mH

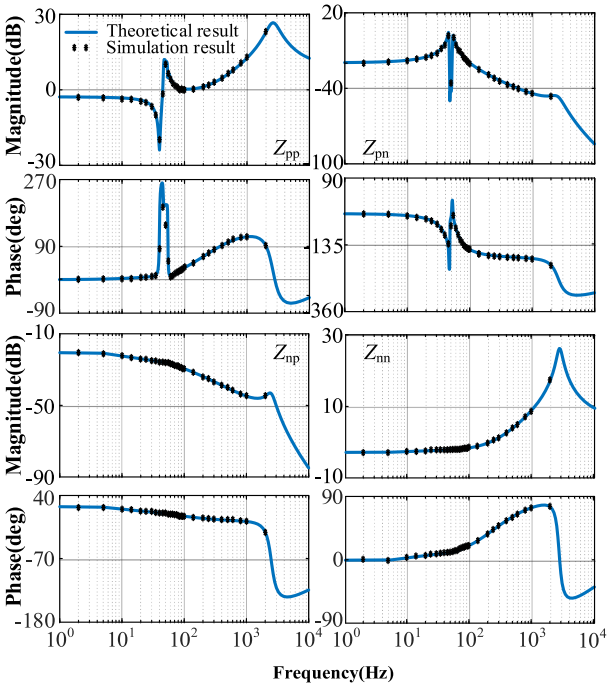

Fig. 3. Frequency responses of output impedance.

phase fluctuation at the fundamental frequency, which might lead to insufficient phase margin and destabilize the system.

Fig. 5 compares the frequency responses of different voltage coefficient. It can be observed that the positive- and negative-sequence impedance do not change significantly, while the amplitude in off-diagonal elements is decreased significantly as K increases. This implies that the value of K may affect the frequency-coupling degree of the system and a larger value of K is beneficial to reduce the coupling terms.

Fig. 6 plots the frequency responses of output impedance when k_{pv} is increased from 1 to 5. The amplitude and phase of diagonal impedance near the fundamental frequency are decreased obviously, indicating that an excessive k_{pv} may contribute to the instability of the system.

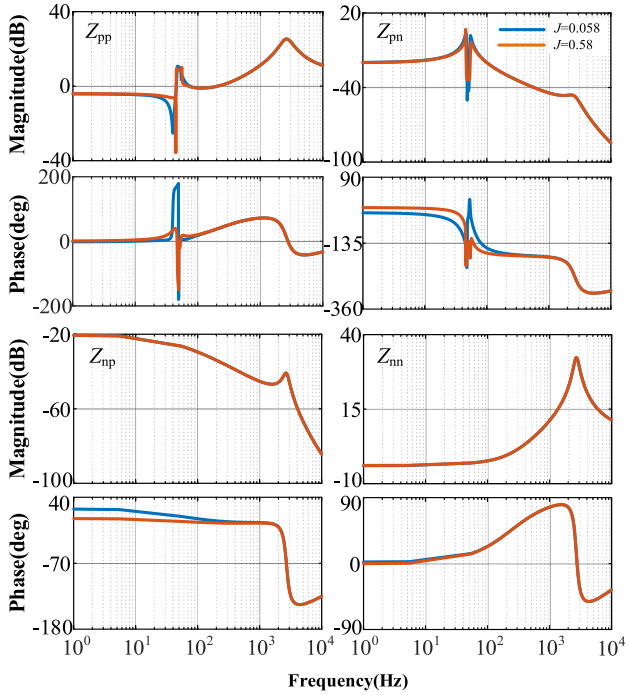

Fig. 4. Frequency responses of output impedance as J changes.

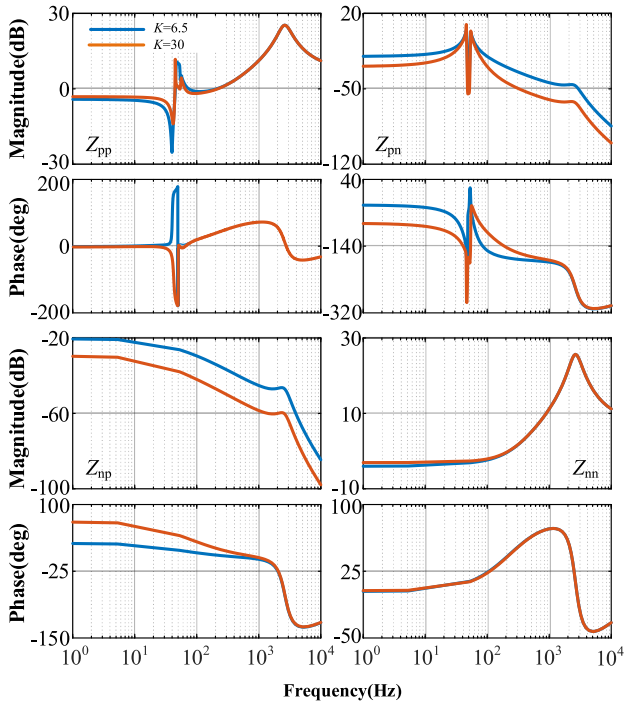

Fig. 5. Frequency responses of output impedance as K changes.

The GNC has been widely applied to the asymmetric impedance matrices for stability analysis [24]. Considering the off-diagonal elements in the admittance matrix, the impedance ratio is given by

$$\mathbf{L}(s) = \mathbf{Y}_{\mathrm{PN}}(s)\,\mathbf{Z}_g(s) \tag{52}$$

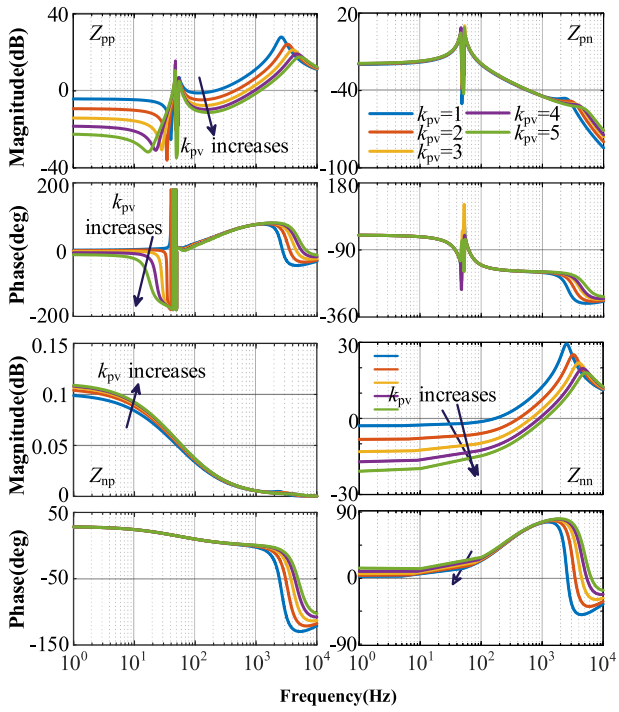

Fig. 6. Frequency responses of output impedance as k_{pv} increases.

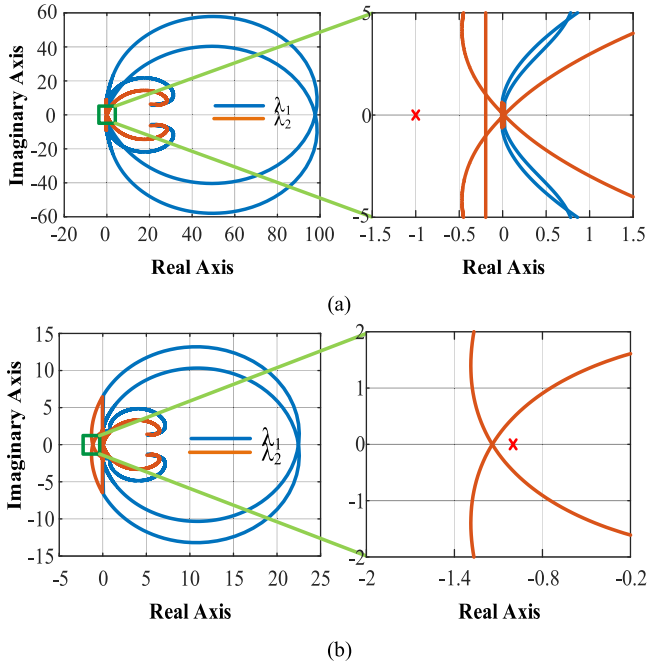

Fig. 7. Nqyuist diagrams for the eigenvalues of $\mathbf{L}(s)$ as L_{g} changes. (a) $L_{\mathrm{g}} =$ 0.01 H. (b) $L_{\mathrm{g}} = 0.002$ H.

where $\mathbf{Z}_{\mathrm{g}}(s) = \mathrm{diag}\{j2\pi(f_{\mathrm{p}}+f_1)L_{\mathrm{g}}, j2\pi(f_{\mathrm{p}}-f_1)L_{\mathrm{g}}\}$.

Fig. 7 compares Nyquist diagrams of the eigenvalues of $\mathbf{L}(s)$ with different SCRs. It can be observed that the characteristic loci encircle $(-1+j0)$ when L_{v} decreases from 10mH (SCR = 6.5) to 2mH (SCR = 33), indicating the system is unstable.

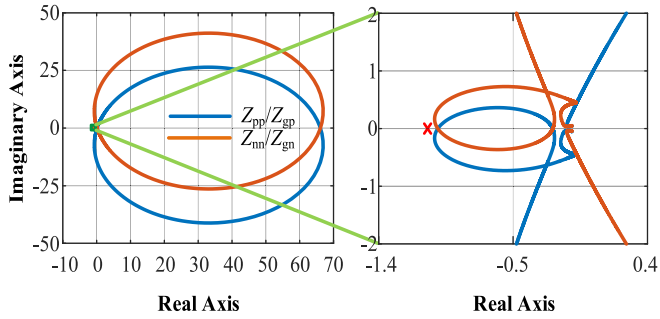

Fig. 8. Nqyuist diagrams for impedance ratios when $L_{\mathrm{g}} = 0.002$ H.

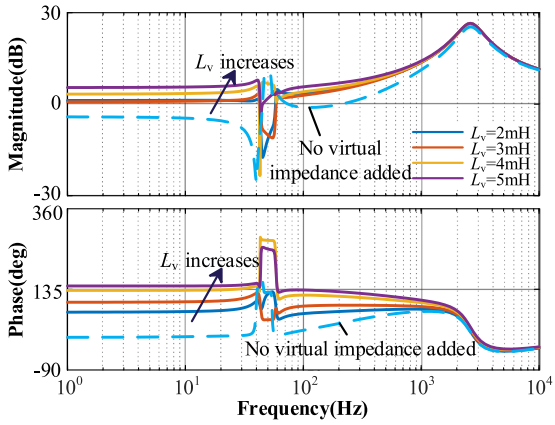

Fig. 9. Frequency responses of $Z_{\mathrm{pp}}(s)$ after adding virtual impedance.

If the frequency-coupling characteristics in VSG are ignored, the positive- and the negative-sequence impedance are mutually decoupled. In this case, the impedance ratio is the grid impedance divided by the output impedance [25]. The Nyquist plots of impedance ratio are shown in Fig. 8. It can be seen that the Nyquist curves are not bypassed (-10), indicating that the system can operate stably. This conclusion is contrary to that in Fig. 7(b). The analysis using the existing model fails to predict instability, as the couplings are neglected. It is revealed that the coupling terms has great significance for stability analysis.

Fig. 9 shows the frequency responses of positive-sequence impedance when virtual impedance is added to the VSG. It is clear that there is a significant increase in the amplitude and phase of the VSG, and this trend becomes more obvious as L_{v} increases. Hence, the addition of virtual impedance is beneficial to enhance the robustness of the system. Nevertheless, the excessive virtual inductor will degrade the decoupling performance. Experiments have verified that there exists a threshold grid inductance ($\mathrm{x_{g\cdot cr}}$). And virtual inductor is not needed when $\mathrm{x_g} > \mathrm{x_{g\cdot cr}}$ [26]. Therefore, comprehensive consideration should be given.

The time-domain simulations of PCC voltage and current are shown in Fig. 10. Two sets of proportionality coefficient, i.e., $k_{\mathrm{pv}} = 1$ and $k_{\mathrm{pv}} = 5$, are tested in Fig. 10(a) and (b). It is clear that the voltage and current are distorted when k_{pv} is increased to 5, which closely correlate with the simulation results in Fig. 6. When L_{g} is decreased to 2mH, the waveform

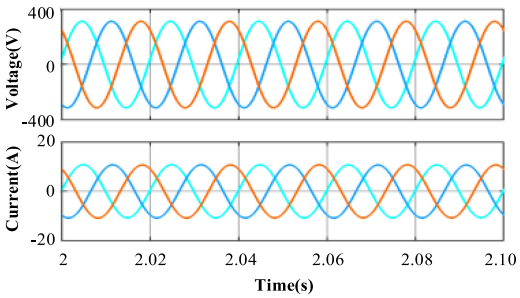

(a) k_{pv}=1.2, L_g=10 mH, L_v=0, K=6.5

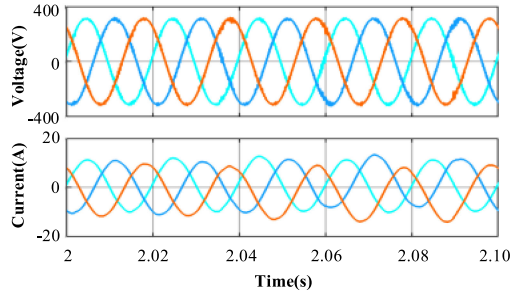

(b) k_{pv}=5, L_g=10 mH, L_v=0, K=6.5

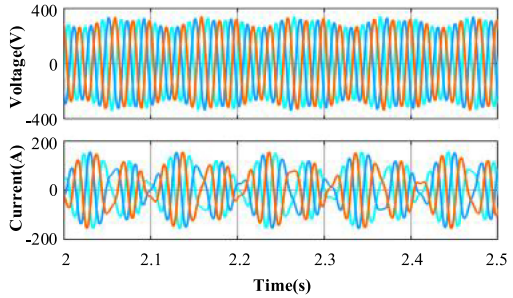

(c) k_{pv}=1.2, L_g=2 mH, L_v=0, K=6.5

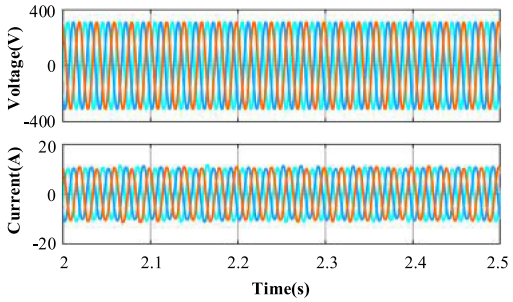

(d) k_{pv}=1.2, L_g=2 mH, L_v=4 mH, K=6.5

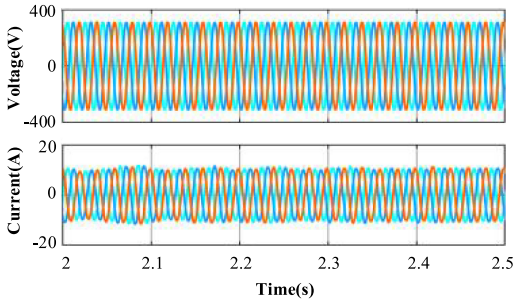

(e) k_{pv}=1.2, L_g=2 mH, L_v=0, K=30

Fig. 10. Simulated PCC voltage and current under different cases.

in Fig. 10(c) shows an unstable operation, matching with the simulation result in Fig. 7(b). After adding virtual impedance, the waveform in Fig. 10(d) has been greatly improved. As shown in Fig. 10(e), raising the value of K has the similar effect due to the decrease of the couplings. The time-domain simulations are consistent with the stability analysis above.

VI. Conclusion

The MFE in VSG was discussed in this paper, and the sequence impedance model of VSG was established based on harmonic linearization, which covered every detail of both power loops and control scheme. The mathematical relationships between different control parameters and the output impedance were revealed. With the help of the analytical model, this paper adopted the impedance responses and GNC to analyze the stability of the VSG. And the following conclusions were drawn:

1) The MFE in VSG has great significance for stability analysis and cannot be ignored. The sequence impedance model with considering couplings is more precise and can predict the exact stability boundary.
2) As the SCR of the system increases, the system is prone to instability.
3) The addition of virtual impedance can increase the amplitude and phase of the diagonal elements obviously, while has no effects on off-diagonal elements. Therefore, it is beneficial to enhance the robustness of the system.
4) There is a close relationship between the power controllers and the MFE, and the variation of control parameters (eg, the virtual moment of inertia J and voltage coefficient K, which are the kernel parameters in VSG) will affect the frequency-coupling degree of VSG.

References

[1] F. Milano, F. Dörfler, G. Hug, D. J. Hill, and G. Verbič, "Foundations and challenges of low-inertia systems (Invited paper)," in *Proc. Power Syst. Comput. Conf.*, 2018, pp. 1–25.
[2] Q. Peng, Q. Jiang, Y. Yang, T. Liu, H. Wang, and F. Blaabjerg, "On the stability of power electronics-dominated systems: Challenges and potential solutions," *IEEE Trans. Ind. Appl.*, vol. 55, no. 6, pp. 7657–7670, Nov./Dec. 2019.
[3] J. Fang, H. Li, Y. Tang, and F. Blaabjerg, "On the inertia of future more-electronics power systems," *IEEE J. Emerg. Sel. Top. Power Electron.*, vol. 7, no. 4, pp. 2130–2146, Dec. 2019.
[4] J. Driesen and K. Visscher, "Virtual synchronous generators," in *Proc. IEEE Power Energy Soc. Gen. Meeting-Convers. Del. Elect. Energy 21st Century*, 2008, pp. 1–3.
[5] Z. Tianwen *et al.*, "Multi-mode operation control for photovoltaic virtual synchronous generator considering the dynamic characteristics of primary source," *Proc. CESS*, vol. 37, no. 2, pp. 454–464, 2017.
[6] D. Chen, Y. Xu, and A. Q. Huang, "Integration of DC microgrids as virtual synchronous machines into the AC grid," *IEEE Trans. Ind. Electron.*, vol. 64, no. 9, pp. 7455–7466, Sep. 2017.
[7] M. F. M. Arani and E. F. El-Saadany, "Implementing virtual inertia in DFIG-based wind power generation," *IEEE Trans. Power Syst.*, vol. 28, no. 2, pp. 1373–1384, May 2013.
[8] D. Yang, H. Wu, X. Wang, and F. Blaabjerg, "Suppression of synchronous resonance for VSGs," *J. Eng.*, vol. 2017, no. 13, pp. 2574–2579, 2017.
[9] S. Dong and Y. C. Chen, "Adjusting synchronverter dynamic response speed via damping correction loop," *IEEE Trans. Energy Convers.*, vol. 32, no. 2, pp. 608–619, Jun. 2017.

[10] G. Li *et al.*, "Analysis and mitigation of subsynchronous resonance in series-compensated grid-connected system controlled by a virtual synchronous generator," *IEEE Trans. Power Electron.*, vol. 35, no. 10, pp. 11096–11107, Oct. 2020.
[11] H. Xin, L. Huang, L. Zhang, Z. Wang, and J. Hu, "Synchronous instability mechanism of P-f droop-controlled voltage source converter caused by current saturation," *IEEE Trans. Power Syst.*, vol. 31, no. 6, pp. 5206–5207, Nov. 2016.
[12] S. D'Arco, J. A. Suul, and O. B. Fosso, "Small-signal modelling and parametric sensitivity of a virtual synchronous machine," in *Proc. Power Syst. Comput. Conf.*, 2014, pp. 1–9.
[13] A. Rodríguez-Cabero, J. Roldán-Pérez, and M. Prodanovic, "Virtual impedance design considerations for virtual synchronous machines in weak grids," *IEEE J. Emerg. Sel. Top. Power Electron.*, vol. 8, no. 2, pp. 1477–1489, Jun. 2020.
[14] S. Wang, Z. Liu, and J. Liu, "Modeling of D-Q small-signal impedance of virtual synchronous generator," in *Proc. IEEE Int. Power Electron. Appl. Conf. Expo.*, 2018, pp. 1–6.
[15] L. Wenbing, W. Jianhua, S. Jingyu, L. Fangfang, G. Shang, and W. Zaijun, "Full-band output impedance model of virtual synchronous generator in dq framework," in *Proc. Int. Power Electron. Conf.*, 2018, pp. 1282–1288.
[16] M. Cespedes and J. Sun, "Impedance modeling and analysis of grid-connected voltage-source converters," *IEEE Trans. Power Electron.*, vol. 29, no. 3, pp. 1254–1261, Mar. 2014.
[17] W. Wu *et al.*, "Sequence impedance modeling and stability comparative analysis of voltage-controlled VSGs and current-controlled VSGs," *IEEE Trans. Ind. Electron.*, vol. 66, no. 8, pp. 6460–6472, Aug. 2019.
[18] Y. Peng, T. Yin, M. Li, Y. Wang, D. Hu, and Z. Liu, "A sequence impedance modeling of VSG with consideration of inner loops control," in *Proc. 4th IEEE Workshop Electron. Grid (eGRID)*, China, 2019, pp. 1–5.
[19] A. Rygg, M. Molinas, C. Zhang, and X. Cai, "A modified sequence-domain impedance definition and its equivalence to the dq-domain impedance definition for the stability analysis of AC power electronic systems," *IEEE J. Emerg. Sel. Top. Power Electron.*, vol. 4, no. 4, pp. 1383–1396, Dec. 2016.
[20] B. Wen, D. Boroyevich, P. Mattavelli, Z. Shen, and R. Burgos, "Experimental verification of the generalized nyquist stability criterion for balanced three-phase ac systems in the presence of constant power loads," in *Proc. IEEE Energy Convers. Congr. Expo.*, 2012, pp. 3926–3933.
[21] W. Liu, Z. Lu, X. Wang, and X. Xie, "Frequency-coupled admittance modelling of grid-connected voltage source converters for the stability evaluation of subsynchronous interaction," *IET Renewable Power Gener.*, vol. 13, no. 2, pp. 285–295, 2018.
[22] S. Shah and L. Parsa, "On impedance modeling of single-phase voltage source converters," in *Proc. IEEE Energy Convers. Congr. Expo.*, 2016, pp. 1–8.
[23] Y. Jiang and A. Ekstrom, "General analysis of harmonic transfer through converters," *IEEE Trans. Power Electron.*, vol. 12, no. 2, pp. 287–293, Mar. 1997.
[24] R. Burgos, D. Boroyevich, F. Wang, K. Karimi, and G. Francis, "On the ac stability of high power factor three-phase rectifiers," in *Proc. IEEE Energy Convers. Congr. Expo.*, 2010, pp. 2047–2054.
[25] J. Sun, "Impedance-Based stability criterion for grid-connected inverters," *IEEE Trans. Power Electron.*, vol. 26, no. 11, pp. 3075–3078, Nov. 2011.
[26] T. Wen, X. Zou, D. Zhu, X. Guo, L. Peng, and Y. Kang, "Comprehensive perspective on virtual inductor for improved power decoupling of virtual synchronous generator control," *IET Renewable Power Gener.*, vol. 14, no. 4, pp. 485–494, Apr. 2019.

Kai Shi was born in Suzhou, China, in 1980. He received the B.S. degree in automation, the M.S. degree in power electronic and power transmission from Jiangsu University, Zhenjiang, China, in 2002 and 2005, respectively, and the Ph.D. degree in power electronic and power transmission from the Nanjing University of Aeronautics and Astronautics, Nanjing, China, in 2012. Since 2002, he has been with the School of Electrical and Information Engineering, Jiangsu University. Since 2013, he has been an Assistant Professor with the Jiangsu University. His current research interests include wind power generator control, grid-connected control, and control strategies of low-voltage ride through.

Yu Wang was born in Suqian, China, in 1995. He received the B.S. degree in electrical engineering and automation from the Jiangsu University, Wuxi, China, in 2018. Since 2018, he has been a Graduate Student with the School of Electrical and Information Engineering, Jiangsu University, Zhenjiang, China. His research interests include power system modeling, stability and control.

Yuxin Sun was born in Taizhou, China, in 1968. She received the M.S. and Ph.D. degrees in electrical engineering from Jiangsu University, Zhenjiang, China. Since 1993, she has been with the School of Electrical and Information Engineering, Jiangsu University. Since 2017, she has been a Professor with the Jiangsu University. Her current research interests include bearingless induction motor control, power generator control, distributed power systems.

Peifeng Xu was born in Nantong, China, in 1980. She received the B.S. and M.S. degrees in electrical engineering from Jiangsu University, Zhenjiang, China, in 2002 and 2005, respectively. Since 2002, she has been with the School of Electrical and Information Engineering, Jiangsu University, Zhenjiang, China. Since 2007, she has been a Lecturer with Jiangsu University. Her current research interests include the design and control of high-efficiency wind power generators.

Feng Gao was born in Taizhou, China, in 1996. He received the B.S. degree in electrical engineering and automation from Jingjiang College, Jiangsu University, Zhenjiang, China, in 2019. Since 2019, he has been a Graduate Student with the School of Electrical and Information Engineering, Jiangsu University, Zhenjiang, China. His research interests include the stability analysis of VSG under unbalanced gird.